

Adding Long-Wavelength Power to N-body Simulations

Shaun Cole

Department of Physics, University of Durham, Science Laboratories, South Rd, Durham DH1 3LE.
 Shaun.Cole@durham.ac.uk

5 February 2020

ABSTRACT

Tormen & Bertschinger have presented an algorithm which allows the dynamic range of N-body simulations to be extended by adding long-wavelength power to an evolved N-body simulation. This procedure is of considerable interest as it will enable mock galaxy catalogues to be constructed with volumes as larger as those of the next generation of galaxy redshift surveys. Their algorithm, however, neglects the coupling between long-wavelength linear modes and short-wavelength non-linear modes. The growth of structure on small scales is coupled to the amplitude of long-wavelength density perturbations via their effect on the local value of the density parameter Ω_0 . The effect of neglecting this coupling is quantified using a set of specially tailored N-body simulations. It is shown that the large-scale clustering of objects defined in the evolved density field such as galaxy clusters is strongly underestimated by their algorithm. An adaptation to their algorithm is proposed that, at the expense of additional complexity, should remedy the shortcomings of the original one. Methods of constructing biased mock galaxy catalogues which utilise the basic algorithm of Tormen & Bertschinger, but avoid the pitfalls are discussed.

Key words: cosmology: theory – large-scale structure of Universe

1 INTRODUCTION

Tormen & Bertschinger (1996) have presented a procedure to extend the dynamic range of large cosmological N-body simulations. Their algorithm allows a periodic N-body simulation in a box of side $S \gtrsim 100h^{-1}\text{Mpc}$ to be replicated and distorted to produce a particle distribution in a larger box of side $L \gtrsim 800h^{-1}\text{Mpc}$, in which the required linear power spectrum is accurately represented in the mass distribution up to wavelengths $\lambda = L$. This procedure can therefore be used to take N-body simulations which have the mass resolution to resolve small galaxy groups and from them construct mock galaxy catalogues equal in volume to the next generation of redshift surveys, *e.g.* the Anglo-Australian 2df galaxy redshift survey (Maddox *et al.* in preparation; <http://msowww.anu.edu.au/colless/2dF/>) and the SDSS (Gunn 1995). Their method, however, neglects coupling between long-wavelength linear modes and short-wavelength non-linear modes. This coupling has only a small effect on the large scale clustering properties of the mass distribution, but a much larger effect on the large scale clustering of non-linear objects such as galaxies or galaxy clusters. In this paper we quantify the effect of neglecting this particular form of mode coupling and suggest how the algorithm could be improved or its shortcomings circumvented.

In Section 2 we present the details of the algorithm used to add long-wavelength power to an N-body simula-

tions. A version of the basic algorithm developed by Tormen & Bertschinger (1996) is detailed in Section 2.1. The effect of long-wavelength linear modes on the evolution of short-wavelength non-linear modes is discussed in Section 2.2, where a modification of the basic algorithm is proposed that at the expense of additional complexity incorporates, to first order, the effect of this form of mode coupling. In Section 3 we use a set of specially tailored N-body simulations to test the basic algorithm and illustrate the effect of ignoring mode coupling. In Section 4 we address the specific problem of constructing large mock galaxy catalogues in which galaxies are biased tracers of the mass distribution. We show how the shortcomings of the basic algorithm can be largely circumvented by restriction to a particular class of biasing scheme. We conclude in Section 5.

2 ADDING LONG-WAVELENGTH POWER

The procedure described by Tormen & Bertschinger (1996) and named MAP (Mode Adding Procedure) consists of the following steps. First the power in long-wavelength modes is removed from the original N-body particle positions and velocities. This new particle distribution is then replicated to define a particle distribution over a much larger volume than that of the original simulation. A new density field is then generated with the required power spectrum on a finer

grid in \mathbf{k} -space, but populating the same physical region of \mathbf{k} -space as the original modes that were removed. The displacements computed from this grid are then used to perturb the replicated particle positions and velocities.

An implementation of these steps is described in Section 2.1, while an additional procedure to deal with the mode coupling not considered by Tormen & Bertschinger (1996) is described in Section 2.2.

2.1 Basic Algorithm: Spatial Perturbations

The starting point of the MAP are the final positions, \mathbf{x} , and velocities, \mathbf{v} , of a large periodic N-body simulation. The size of the box, S , must be greater $\sim 100h^{-1}\text{Mpc}$ so that the evolution of the longest wavelength modes present in the box is still described well by linear theory. One also requires the corresponding linear density field, $\delta^S(\mathbf{x})$, but since only the long-wavelength contribution to this field is used this can be computed accurately from the particle positions.

The first step is to compute the long-wavelength contribution, $\Delta^S(\mathbf{x})$, to the density field $\delta^S(\mathbf{x})$. This is achieved by Fourier transforming the density field and then constructing $\Delta^S(\mathbf{x})$ using only the long-wavelength Fourier modes,

$$\Delta^S(\mathbf{x}) = \sum_{l,m,n} \delta_k^S e^{i\mathbf{k}\cdot\mathbf{x}} \quad (2.1)$$

where $\mathbf{k} = (2\pi/S)(l, m, n)$ and $-N_S \leq l, m, n \leq N_S$. The extent of the region of \mathbf{k} -space defining $\Delta^S(\mathbf{x})$ (chosen here for simplicity to be a cube) should be limited such that $\langle |\Delta^S(\mathbf{x})|^2 \rangle \ll 1$. It is this constraint that determines N_S and thus the number of modes that are removed and later resampled. In practice the algorithm works accurately provided $\langle |\Delta^S(\mathbf{x})|^2 \rangle^{1/2} \lesssim 0.2$. The next step is to compute the displacements produced by these modes using the Zel'dovich (1970) approximation,

$$\mathbf{d}^S(\mathbf{x}) = \sum_{l,m,n} \frac{\delta_k^S \mathbf{k}}{k^2} e^{i\mathbf{k}\cdot\mathbf{x}}. \quad (2.2)$$

These displacements are readily computed on a grid using an FFT. The removal of long-wavelength power from the N-body simulation is then achieved by subtracting these displacements from the final N-body particle positions

$$\mathbf{x}' = \mathbf{x} - \mathbf{d}^S(\mathbf{x}) \quad (2.3)$$

and velocities

$$\mathbf{v}' = \mathbf{v} - f(\Omega) \mathbf{d}^S(\mathbf{x}). \quad (2.4)$$

Here $f(\Omega)$ is the logarithmic derivative of the linear growth factor $D(a)$ with respect to the expansion factor a and if we use the convention that positions are measured in units of $h^{-1}\text{Mpc}$ then the velocities are in units of 100km s^{-1} . Note that the value of the field $\mathbf{d}^S(\mathbf{x})$ needs to be smoothly interpolated from the grid on which it is defined to each particle position.

Normally, when using the Zel'dovich approximation for a particle at position \mathbf{x} , one computes the displacement $\mathbf{d}^S(\mathbf{q})$ evaluated at the Lagrangian or starting position, \mathbf{q} , of that particle. Here instead we have deliberately computed the displacement $\mathbf{d}^S(\mathbf{x})$ at the final position \mathbf{x} . For this reason the above procedure to remove the long-wavelength power is not exact. However, provided the displacements

$\mathbf{d}^S(\mathbf{x})$ are small compared to the wavelength of the modes comprising $\Delta^S(\mathbf{x})$ the difference between $\mathbf{d}^S(\mathbf{q})$ and $\mathbf{d}^S(\mathbf{x})$ is small and approximation works quite accurately. This constraint is identical to requiring $\langle |\Delta^S(\mathbf{x})|^2 \rangle \ll 1$, as $\Delta^S(\mathbf{x}) = \nabla \cdot \mathbf{d}^S(\mathbf{x})$, and so is well satisfied in all cases of interest. Tormen & Bertschinger (1996) describe a more elaborate and accurate method of removing the long-wavelength power. The reason for deliberately using $\mathbf{d}^S(\mathbf{x})$ in equations (2.3) and (2.4) is that we do not wish to disturb the small scale structure of the N-body simulation. For example, we wish the effect of the displacement field on a dense virialized cluster to be to move the whole cluster but not disrupt its internal structure. Thus the variation of displacement $\mathbf{d}^S(\mathbf{x})$ across the cluster should be small. With the above formulation this occurs naturally as the cluster particles span only a small range in \mathbf{x} , but the shear would be considerably larger if $\mathbf{d}^S(\mathbf{q})$ were used since the cluster particles would span a much larger volume in the initial Lagrangian space.

The simulation, now with no power in long-wavelength modes, is replicated to define particle positions and velocities in a much larger box of side $Lh^{-1}\text{Mpc}$. It is convenient to make L an odd multiple of S so that in \mathbf{k} -space the two grids have cells whose boundaries are aligned. A new Gaussian random field is generated from the required power spectrum

$$\Delta^L(\mathbf{x}) = \sum_{l,m,n} \delta_k^L e^{i\mathbf{k}\cdot\mathbf{x}} \quad (2.5)$$

where $\mathbf{k} = (2\pi/L)(l, m, n)$ and $-N_L \leq l, m, n \leq N_L$ with $2N_L + 1 = (2N_S + 1)(L/S)$. Note that the sampling of \mathbf{k} -space is now on a much finer grid than for $\Delta^S(\mathbf{x})$. The corresponding Zel'dovich approximation displacements, defined over the whole box of size $Lh^{-1}\text{Mpc}$, are given by

$$\mathbf{d}^L(\mathbf{x}) = \sum_{l,m,n} \frac{\delta_k^L \mathbf{k}}{k^2} e^{i\mathbf{k}\cdot\mathbf{x}}. \quad (2.6)$$

These are then simply added to the previous positions and velocities,

$$\mathbf{x}'' = \mathbf{x}' + \mathbf{d}^L(\mathbf{x}') \quad (2.7)$$

$$\mathbf{v}'' = \mathbf{v}' + f(\Omega) \mathbf{d}^L(\mathbf{x}') \quad (2.8)$$

to produce a particle distribution with the required improved sampling of long-wavelength modes.

2.2 Temporal Perturbations

The MAP detailed in Section 2.1 assumes that there is no coupling between long-wavelength linear modes and short-wavelength non-linear modes beyond that contained implicitly in the Zel'dovich approximation. The coupling contained in the Zel'dovich approximation occurs as long-wavelength modes produce a wave of expansion/compression which modulates the frequencies of all shorter wavelength modes. These same long-wavelength modes also couple to shorter wavelengths through the way they perturb the evolution of small scale structure. To first order the addition of a long-wavelength density perturbation, Δ , can be thought of as a perturbation in the value of the density parameter from Ω_0 to $\Omega_0(1 + \Delta)$. This perturbation to Ω_0 causes a corresponding perturbation in the linear growth rate of density fluctuations, $D(a, \Omega_0, \Lambda_0)$, in that region. Since the growth factor is

also a function of time, or expansion factor, this perturbation can be thought of as a temporal perturbation. Namely, in a region where one is adding a long-wavelength density perturbation, Δ , the simulation should be allowed to evolve longer to the point where $D(a'', \Omega_0, \Lambda_0) = D(a, \Omega_0(1 + \Delta), \Lambda_0)$. Thus, expanding both sides of this equation in a Taylor series, to first order, the temporal perturbation can be related to the density perturbation by

$$a'' = a \frac{(1 + \Delta)}{f(\Omega)} \left(\frac{d \ln D}{d \ln \Omega} \right)_{a, \Lambda_0} \quad (2.9)$$

where $\Delta(\mathbf{x}) = \Delta^L(\mathbf{x}) - \Delta^S(\mathbf{x})$. For $\Lambda_0 = 0$ this reduces to

$$a'' \approx a(1 + \Delta) \frac{(1 - \Omega_0^{0.6})}{(1 - \Omega_0)\Omega_0^{0.6}} \quad (2.10)$$

where the usual approximation $f(\Omega) \approx \Omega^{0.6}$ (e.g. Peebles 1993) has been made.

If for the smooth fields $\mathbf{d}^S(\mathbf{x})$, $\Delta^S(\mathbf{x})$, $\mathbf{d}^L(\mathbf{x})$ and $\Delta^L(\mathbf{x})$ we ignore the difference in their values at $\mathbf{x}(a)$, $\mathbf{x}'(a)$ and $\mathbf{x}(a'')$ we can combine this operation and that described in Section 2.1 into a single operation. The new particle positions and velocities are given by

$$\mathbf{x}''(a) = \mathbf{x}(a'') + \mathbf{d}(\mathbf{x}(a)) \quad (2.11)$$

$$\mathbf{v}''(a) = \mathbf{v}(a'') + f(\Omega_0)\mathbf{d}(\mathbf{x}(a)) \quad (2.12)$$

where a'' is given by (2.9) with $\mathbf{d}(\mathbf{x}) = \mathbf{d}^L(\mathbf{x}) - \mathbf{d}^S(\mathbf{x})$. The practical problem with this procedure is that the N-body particle distributions are now required not just at one single output time but over a quite extended range. An efficient implementation would probably require merging the code to carry out this transformation with the basic N-body evolution code so that individual particle positions and velocities are only output at the required times.

3 COMPARISON WITH FULL NON-LINEAR COMPUTATION

To test the effect of neglecting the linear to non-linear mode coupling described in Section 2.2 we now compare two N-body simulations. The first has long-wavelength power added a posteriori using the MAP detailed in Section 2.1, while the second has the long-wavelength power included in the initial conditions prior to being evolved. If the MAP works exactly then the particle distributions in these two simulations should be identical in every respect.

3.1 The Simulations

We first produced a realization of a Gaussian random field on a 64^3 grid with the CDM power spectrum of Bardeen *et al.* (1986) for $\Gamma \equiv \Omega_0 h = 0.25$. We chose the amplitude of the power spectrum such that the linear rms density fluctuation in spheres of radius $8h^{-1}\text{Mpc}$ was $\sigma_8 = 0.5$ at the present day, in agreement with the value required to produce the observed abundance of X-ray clusters (e.g. White, Efstathiou & Frenk 1993; Eke, Cole & Frenk 1996; Viana & Liddle 1996). The physical size of the box was chosen to be $S = 115.2h^{-1}\text{Mpc}$ and the density parameter was taken to be $\Omega_0 = 1$. The only unusual feature about this density field is that we explicitly set to zero the power in the cube

of 27 modes surrounding $\mathbf{k} = 0$. Thus in the terminology of Section 2.1 we choose $N_S = 1$ and explicitly set $\Delta^S(\mathbf{x}) \equiv 0$ in this density field.

This 64^3 density field was then used to generate the initial conditions of two N-body simulations. First the density field was replicated 3^3 times to produce a periodic density field on a 192^3 grid filling a box of side $L = 3S = 345.6h^{-1}\text{Mpc}$. This density field and the Zel'dovich approximation were then used to set up a perturbed grid of 192^3 particles. The simulation evolved from these initial conditions we shall refer to as ‘‘Periodic’’. A second set of initial conditions was generated by adding a density field $\Delta^L(\mathbf{x})$ to the periodic 192^3 density field. Here $\Delta^L(\mathbf{x})$ was a Gaussian random field generated on a 192^3 , but with power only in the inner cube of 9^3 modes. Thus in the terminology of Section 2.1, $N_L = 4$ and the Fourier content of $\Delta^L(\mathbf{x})$ covers exactly that region of \mathbf{k} -space left empty in the original 64^3 density field, but on a grid which is three times finer. For the chosen power spectrum and normalization the rms value of this field is $\langle |\Delta^L(\mathbf{x})|^2 \rangle^{1/2} = 0.19$ at the final time. The simulation run from these initial conditions in which the long-wavelength density field $\Delta^L(\mathbf{x})$ was added to the particle distribution prior to evolution we shall refer to as ‘‘Prior’’. Both simulations were evolved from a starting redshift of $z = 4$ to the present epoch with the AP³M code of Couchman (1991), using a comoving force softening of $\eta = 180h^{-1}\text{kpc}$ (equivalent to a Plummer softening of $\epsilon = 60h^{-1}\text{kpc}$). A third and final particle distribution was then generated from the Periodic simulation using the MAP. This simulation, derived from the Periodic simulation in which the long-wavelength power, $\Delta^L(\mathbf{x})$, was added in after evolution we refer to as ‘‘Post’’.

3.2 The Mass Distribution

We now compare the mass distributions in the Periodic, Prior and Post simulations. We note that although these simulations do not exploit the full potential of the MAP (the replicated volume contains only 64^3 particles and is replicated only 3^3 times) they provide a more direct and stringent test than the simulations compared in Tormen & Bertschinger (1996). To the extent to which MAP works the Post and Prior particle distributions should be identical. Thus we are able to study quite subtle differences between the two simulations that would not have been possible if the two simulations had different phases and differing resolution as was the case in Tormen & Bertschinger (1996).

A visual comparison of the mass distribution in slices through the three simulations is shown in Figs. 1, 2 and 3. The 3-fold periodicity of the Periodic simulation is clearly visible in Fig. 1. The manner in which the MAP distorts this particle distribution and introduces long-wavelength power can be seen by comparing Figs. 1 and 2. The structures visible in Fig. 1 are displaced in a coherent fashion both in and perpendicular to the plane of the plot. The most interesting figures to compare are Figs. 2 and 3 which compare the particle positions in the true or Prior simulation with those synthesised using the MAP. Here we also show close-ups of two selected regions so that the small scale structure in the simulations can be compared in some detail. On first inspection it is impressive how well the Post and Prior distributions agree. The only discernible differences are on very

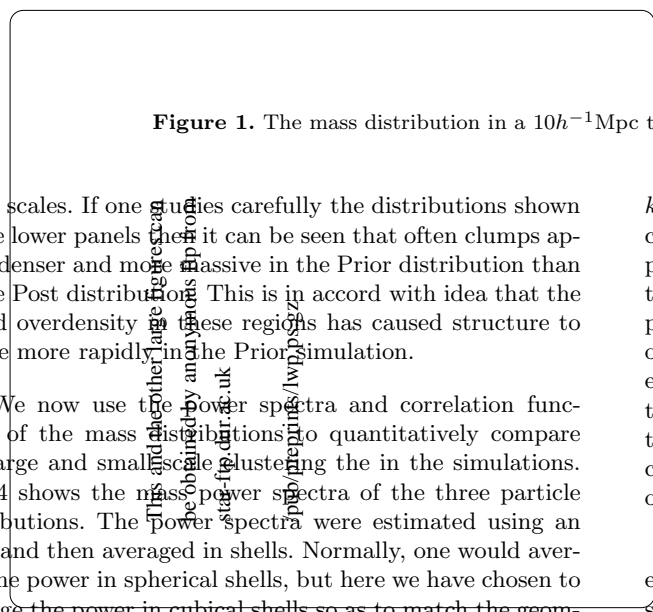


Figure 1. The mass distribution in a $10h^{-1}\text{Mpc}$ thick slice through the Periodic simulation.

small scales. If one studies carefully the distributions shown in the lower panels then it can be seen that often clumps appear denser and more massive in the Prior distribution than in the Post distribution. This is in accord with the idea that the added overdensity in these regions has caused structure to evolve more rapidly in the Prior simulation.

We now use the power spectra and correlation functions of the mass distributions to quantitatively compare the large and small scale clustering in the simulations. Fig. 4 shows the mass power spectra of the three particle distributions. The power spectra were estimated using an FFT and then averaged in shells. Normally, one would average the power in spherical shells, but here we have chosen to average the power in cubical shells so as to match the geometry of the region of \mathbf{k} -space in which the long-wavelength power has been added. (The oscillations present in the equivalent figure (Fig. 8) of Tormen & Bertschinger (1996) have been avoided by rebinning the power into bins whose spacing matches the sampling of \mathbf{k} -space in the initial conditions.) The first thing to note is the sharp drop to zero power at

$k < 0.11h\text{Mpc}^{-1}$ in the case of the Periodic simulation. This corresponds precisely to the region of \mathbf{k} -space in which the power spectrum was set to zero in the initial conditions of the Periodic simulation. At these same long-wavelengths the power spectra of the Post and Prior simulation track each other very accurately and scatter around the required linear theory power spectrum. At higher- k (smaller scales), all three power spectra lie above the linear theory power spectrum. Here the power spectrum of the Post simulation lies closest to that of the Periodic, which is slightly below that of the Prior simulation.

We can study the small structure in more detail by examining the correlation functions of the three simulations shown in Fig. 5. The lack of large scale power in the Periodic simulation can be seen here as a dramatic decrease in $\xi(r)$ for $r \gtrsim 10h^{-1}\text{Mpc}$. The correlation function of the Post simulation agrees well with the Prior simulation on these large scales. At smaller scales, the lower panel shows that the Post correlation function peels away from that of the Prior and matches accurately the correlation function of

The results shown in this figure are obtained by anonymous referee. The referee's name is Steve Fardal, and the URL of the referee's website is <http://www.astro.umd.edu/~fardal/>.

This and the other large figures can be obtained by anonymous ftp from
 star-ftp.dur.ac.uk
 /pub/preprints/lwp.ps.gz

Figure 2. The mass distribution in the same slice as Fig. 1, but for the Post simulation where long-wavelength power has been added to the Periodic simulation using the Tormen & Bertschinger (1996) procedure. The lower panels show two regions of size $50h^{-1}\text{Mpc}$ and $30h^{-1}\text{Mpc}$ taken from this slice on an expanded scale.

the Periodic simulation. This is a convincing demonstration that the MAP has basically worked. The small scale structure in the Periodic Simulation has been undisturbed while at the same time the required large scale power has been generated. The only sign of the neglect of the interaction between large scale linear modes and small scale structure is the slight amount by which $\xi(r)$ for the Periodic and Post simulations lies below that of the Prior simulation at small scales.

3.3 The Distribution of Clusters

Here we examine the clustering of a set of objects which do *not* simply trace the mass distribution, but are instead biased tracers. As an example of such objects we use massive groups or clusters identified in the simulations.

We selected a sample of clusters in each of the simulations using the standard friends-of-friends group finding

algorithm (Davis *et al.* 1985) with a linking length 0.2 times the mean inter-particle separation. This algorithm approximately selects groups with mean overdensity of 200. We then ranked the clusters by mass and retained the 1000 with highest mass in each simulation. This gives a sample of clusters with mean separation of $34h^{-1}\text{Mpc}$ which makes them approximately three times more abundant than Abell $R \geq 1$ galaxy clusters. These cluster samples are shown for the Post and Prior simulations in Fig. 6. In several cases the same cluster are identified in each simulation. There are then many cases where only one member of a close cluster pair in the Post simulation is found in the Prior. However, the most significant difference is the tendency for the large voids in the Prior cluster distribution to be peppered with one or two isolated clusters in the Post distribution. This can result in a large difference in their large scale clustering properties.

We examine the clustering properties of the two cluster

This and the other large figures can be obtained by anonymous ftp from
 star-ftp.dur.ac.uk
 /pub/preprints/lwp.ps.gz

Figure 3. The same as Fig. 2 but for the Prior simulation.

samples in Figs. 7 and 8. The cluster samples are too small to estimate $\xi(r)$ on very small scales. On large scales we see that the cluster correlation function in the Prior simulation is of the same shape as that of the underlying mass distribution but is offset in amplitude. In contrast the cluster correlation function in the Post simulation is considerably weaker. This difference in clustering on large scales is perhaps more clearly seen in Fig 8, which plots the fractional rms variation in the number of clusters in spheres of radius, r , as a function of r .

Another comparison of the properties of the two cluster samples is given by the peculiar velocity distribution shown in Fig. 9. In the Post and Prior simulations the large-scale velocity fields are very almost equal, just as is the large-scale mass distribution. Nonetheless, differences in the peculiar velocity distributions could arise because of the differing way the cluster populations sample the velocity field in the two simulations. The similarity of the Post and Prior distributions shown in Fig. 9 indicate that this is a small effect in this case, but it is hard to dismiss in general. Also note that

the peculiar velocity distribution in the Periodic simulation is much narrower. This demonstrates that long-wavelength modes produce a large contribution to the peculiar velocity and their effect is well modelled using the MAP.

The differences we have found in the properties of the cluster distributions are due to the way long-wavelength modes modulate the cluster abundance and in general the properties of the non-linear density field. In the Prior simulation the cluster abundance is modulated by, and in phase with, the long-wavelength modes in the simulation. In contrast in the Post simulation the cluster abundance is uncorrelated with the long-wavelength modes which are added in after the simulation is evolved.

4 MOCK GALAXY CATALOGUES

The differences that we have noted in the cluster catalogues arise because MAP does not produce the correct correlation between the large-scale density field and the small-scale non-

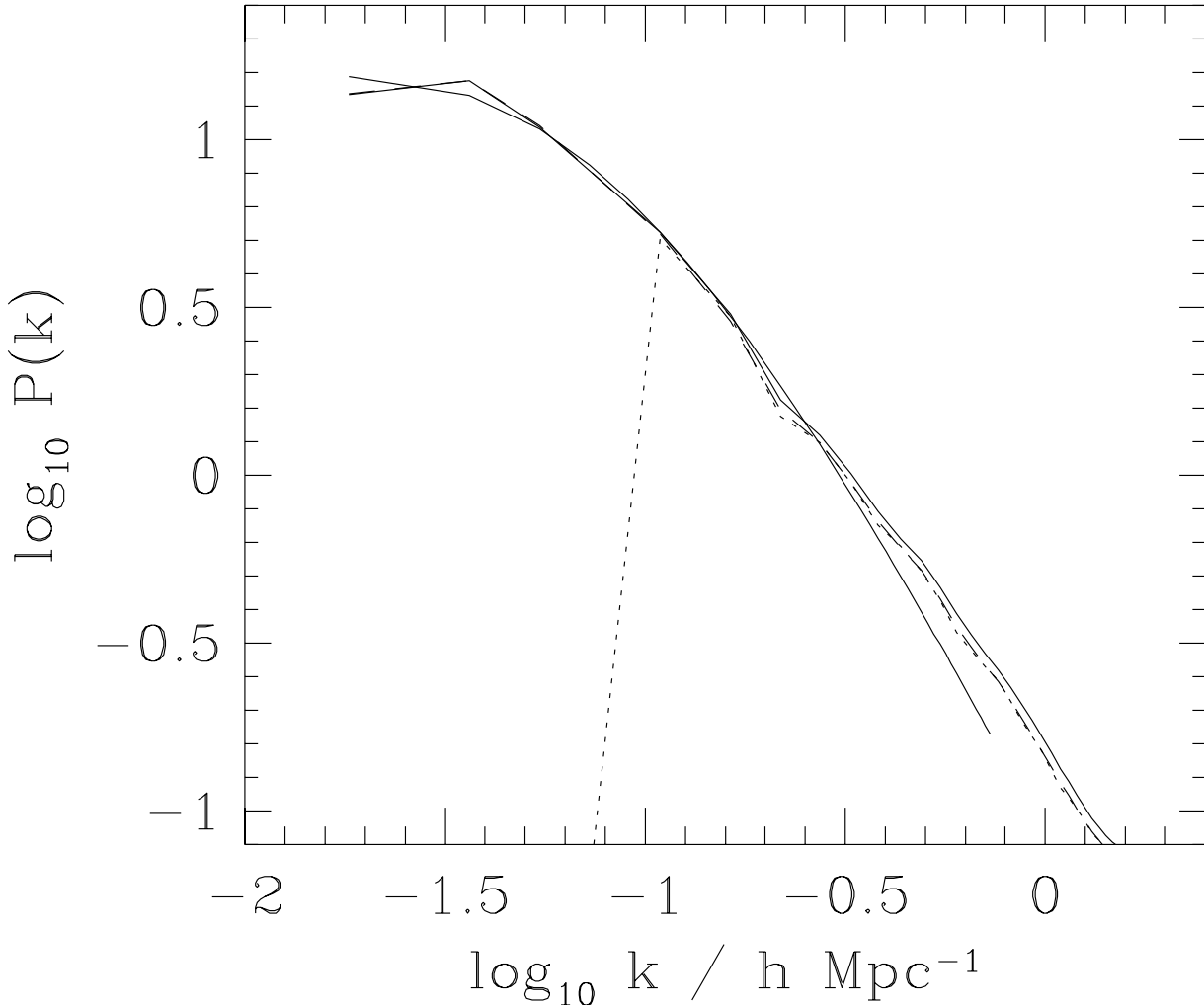


Figure 4. The mass power spectrum, $P(k)$, in the Periodic (dotted), Post (dashed) and Prior (solid) simulations. Note, the dashed curve is coincident with the solid curve at small k , but closer to the dotted curve at high k . The smooth solid curve is the linear theory power spectrum. Each power spectrum has been averaged in cubical shells of side $2k$ and thickness matched to the spacing sampling of \mathbf{k} -space in the initial conditions of the simulations.

linear structure. This results in large differences on large scales for the clusters because the cluster selection is done using the small-scale properties of the non-linear density field. The same problems will also occur when constructing mock galaxy catalogues where the galaxy identification or biasing algorithm is a function of the small-scale non-linear density field. An example of where the resulting error is important is in the determination of the density parameter Ω_0 from redshift space distortions of the clustering pattern (Kaiser 1987). At large scales, in the linear regime, a distortion is expected whose strength is determined by $\Omega_0^{0.6}/b$ and which is independent of scale. For galaxy catalogues constructed from the density produced by MAP the bias parameter b is a decreasing function of scale. Thus in the mock catalogues one would measure a distortion which indicates that $\Omega_0^{0.6}/b$ increases with scale rather than converging to the true value.

These problems with the MAP could be addressed as in Section 2.2 where it is described how the correct correlation between the large-scale density field and small-scale struc-

ture could be generated by using multiple outputs from the evolving N-body simulation. However, a simpler procedure maybe valuable for the specific case of creating mock galaxy catalogues. If galaxies are selected in the *initial* conditions, *i.e.* from the initial density field including the added long-wavelength contribution $\Delta(\mathbf{x}) = \Delta^L(\mathbf{x}) - \Delta^S(\mathbf{x})$, then the main deficiencies of the MAP are by-passed. An example of defining galaxies in the initial conditions, which has been much used, is the peaks biasing scheme (White *et al.* 1987). Here the long-wavelength modes influence the galaxy selection probability through the way they modulate the number density of high peaks in the small scale density field (Bardeen *et al.* 1986). Galaxies selected in this way have an abundance which varies in phase with the long-wavelength modes that are to be added using the MAP. This will result in them having the correct bias on large scales. Thus like the mass distribution the only error in using the MAP is then small and confined to small scales.

Clusters identified in the galaxy distribution will fewer problems than those selected in the mass distribution. As

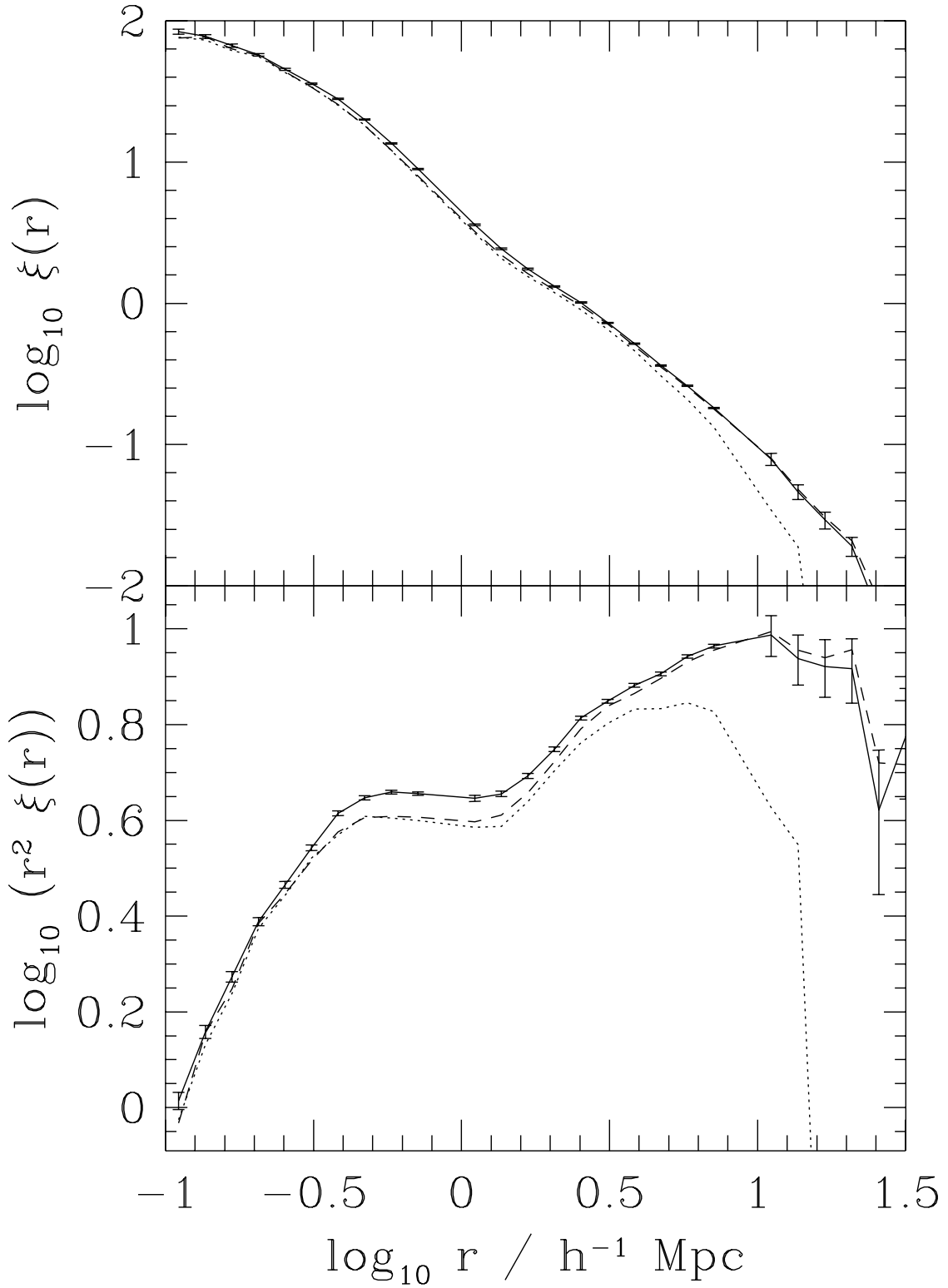


Figure 5. The upper panel show the mass correlation function, $\xi(r)$ estimated from random samples of particles taken from the Periodic (dotted), Post (dashed) and Prior (solid) simulations. Poisson errorbars are indicated on the correlation function of the Prior simulation. The lower panel shows $r^2 \xi(r)$ on an expanded scale so that the differences between the three simulations can be seen more clearly.

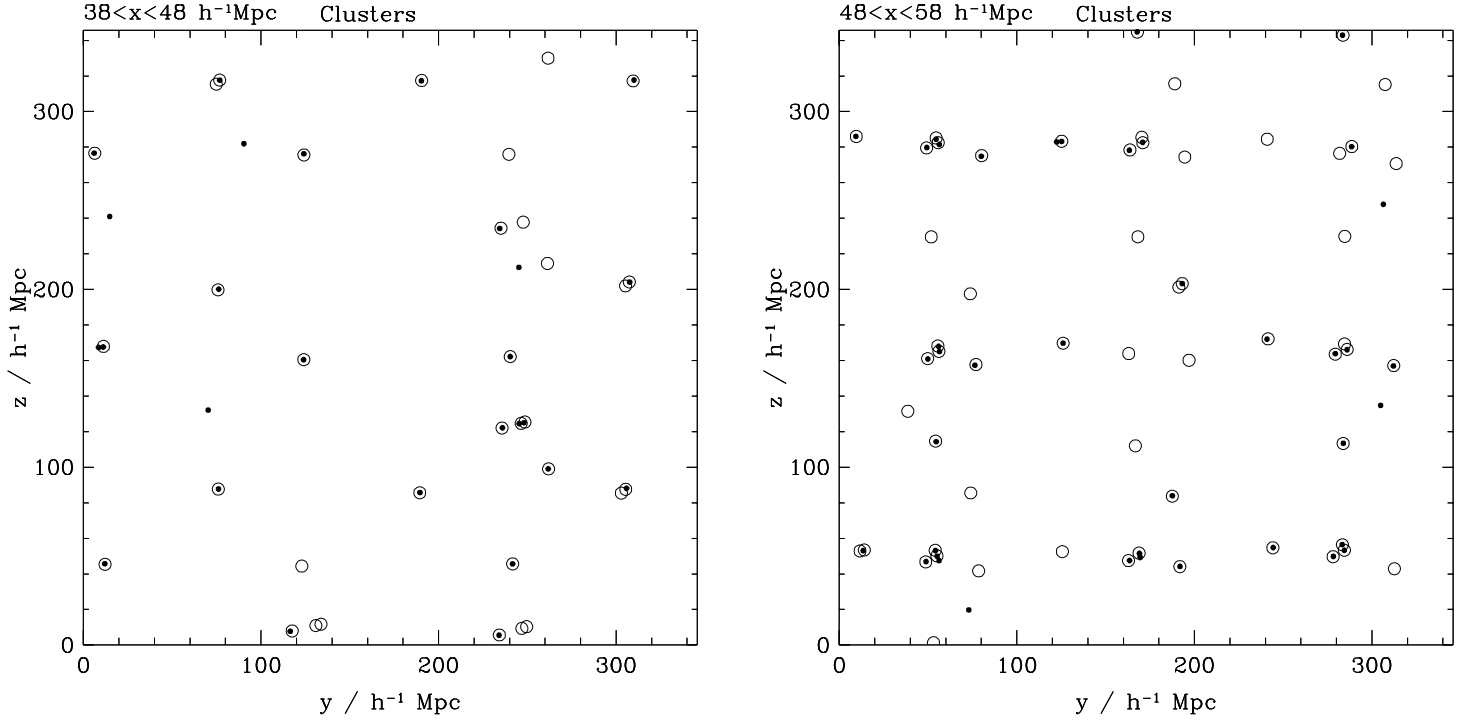


Figure 6. A comparison of the spatial distribution of galaxy clusters as defined by the friends-of-friends group finding algorithm in two slices through the Post (open symbols) and Prior (filled symbols) simulations. Each slice is $10h^{-1}\text{Mpc}$ thick and the left-hand slice is coincident with the slices of the mass distributions shown in Figs. 2 and 3

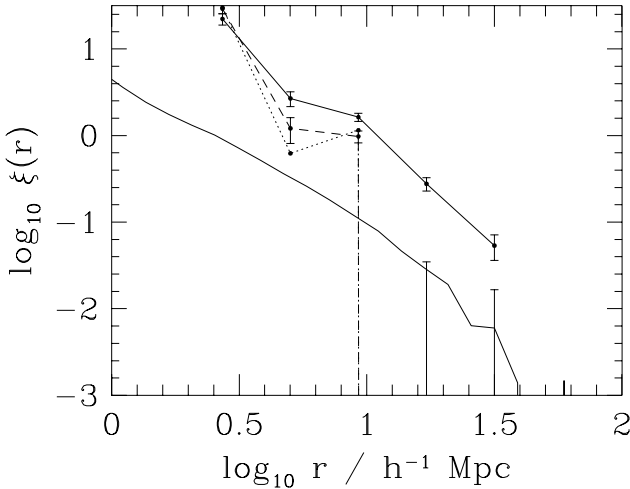


Figure 7. The cluster correlation function, $\xi(r)$, for the Periodic (dotted), Post (dashed) and Prior (solid) simulations. Poisson errorbars are indicated on both the Post and Prior correlation functions. The lower solid line shows the correlation function of the underlying mass distribution taken from the Prior simulation.

discussed in Section 3.3 cluster masses and dynamics should be modified by the addition of long-wavelength power. Here the cluster richesses will be modulated by the added long-wavelength modes via the galaxy selection algorithm, but their small scale dynamics will remain affected and uncorrelated with the added long-wavelength density field.

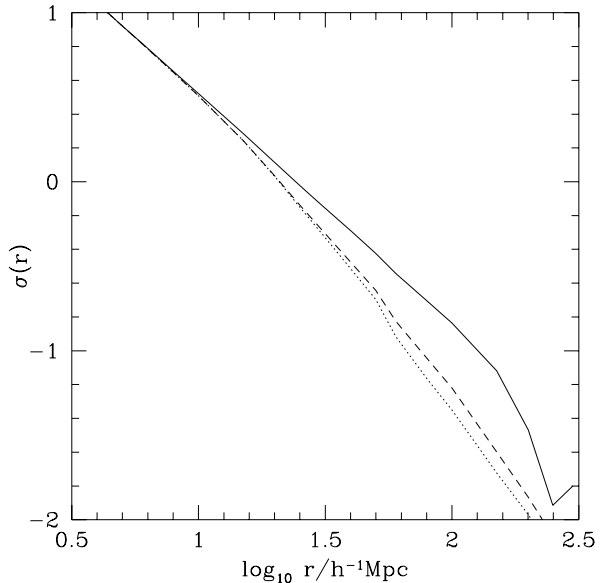


Figure 8. The rms variation, $\sigma(r)$ in the number of clusters in spheres of radius r for the Periodic (dotted), Post (dashed) and Prior (solid) simulations.

5 CONCLUSIONS

The algorithm devised by Tormen & Bertschinger (1996) allows the dynamic range of N-body simulations to be extended to very large scales by adding to them linear power on very large scales. However, the Tormen & Bertschinger

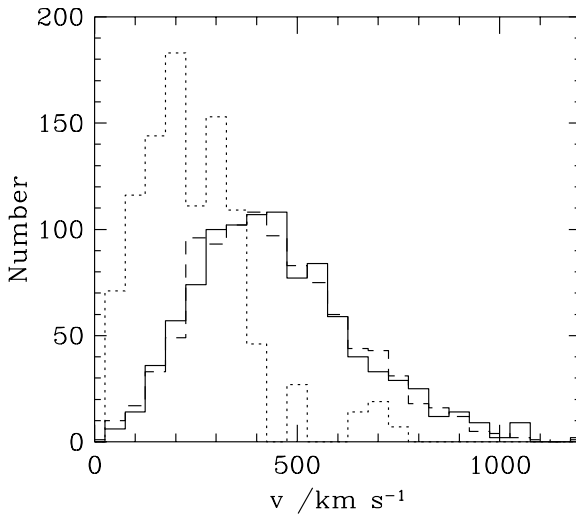


Figure 9. The peculiar velocity distributions in the Periodic (dotted), Post (dashed) and Prior (solid) simulations.

(1996) Mode Adding Procedure (MAP) neglects coupling between long-wavelength linear modes and short-wavelength non-linear modes. This coupling arises through the way long-wavelength density modes modulate the rate of evolution of small structure. Although the amplitude of this effect is small it is of the same order as the amplitude of the long-wavelength density modes. Thus for objects such as galaxies or galaxy clusters identified in the non-linear density field the neglect of this coupling leads to a large error in the amplitude of their large-scale clustering pattern. On the other hand, for the mass distribution as a whole we find the MAP works very accurately with essentially no error in the mass correlation function on large scales and only a small error in the amplitude on small scales.

The main short-comings of the MAP can be avoided by selecting objects in the initial conditions where the initial conditions include the long-wavelength modes that are to be introduced using the MAP of Tormen & Bertschinger (1996). Thus mock galaxy catalogues based on the peaks biasing prescription, or in fact any biasing algorithm which uses only the initial density field, will benefit from the ability of the MAP to better sample modes of the very large scale density field. Alternatively, if one requires the full mass distribution then the Tormen & Bertschinger procedure can be extended to explicitly address the coupling of long-wavelength modes to small scale structure by using multiple outputs from the evolving N-body simulation.

ACKNOWLEDGEMENTS

SMC would like to thank Carlos Frenk for useful discussions and Hugh Couchman for providing a copy of his AP³M N-body code and giving valuable advice. SMC also gratefully acknowledges the support of a PPARC Advanced Fellowship.

REFERENCES

Bardeen, J.M., Bond, J.R., Kaiser, N., Szalay, A.S., 1986, *ApJ*, 304,15
 Couchman, H.M.P., 1991, *ApJ.Lett*, 368,23
 Davis, M., Efstathiou, G., Frenk, C.S., White, S.D.M., 1985, *ApJ*, 292,371
 Eke, V.R. Cole, S. Frenk, C.S., 1996, *MNRAS* submitted.
 Gunn, J.E. 1995 *BAAS*, 186,44
 Kaiser, N., 1987, *MNRAS*, 227,1
 Peebles, P.J.E., 1993, *Principles of Physical Cosmology*. Princeton University Press, Princeton, NJ.
 Tormen , G., Bertschinger, E., 1996, *ApJ*, submitted.
 Viana, P.T.P., Liddle, A.R., 1996, *MNRAS* submitted.
 White, S.D.M., Davis, M., Efstathiou, G., Frenk, C.S., 1987, *Nature*, 330,451
 White, S.D.M., Efstathiou, G., Frenk, C.S. 1993, *MNRAS*, 262,1023
 Zel'dovich Y.B., 1970, *A& A* 5,84